Journal of Materials Chemistry A

Accepted Manuscript

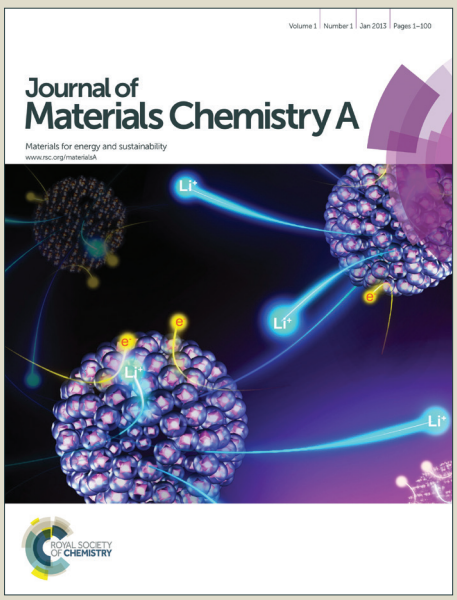

ROYAL SOCIETY OF CHEMISTRY

www.rsc.org/materialsA

Graphical Abstract

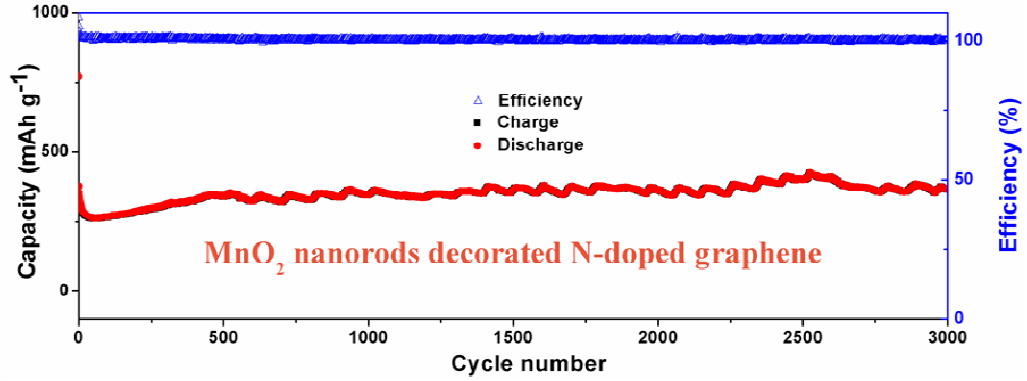

Summary: We report ultralong cycle-life lithium ion batteries based on the nitrogen-doped graphene/MnO_2 hybrids.

A New Approach towards Nitrogen-Doped Graphene/MnO_2 Hybrids for Ultralong Cycle-Life Lithium Ion Batteries

Tingzhou Yang, Tao Qian,* Mengfan Wang, Jie Liu, Jinqiu Zhou, Zhouzhou Sun, Muzi Chen, Chenglin Yan*

College of Physics, Optoelectronics and Energy & Collaborative Innovation Center of Suzhou Nano Science and Technology, Soochow University, Suzhou 215006, China. Email: c.yan@suda.edu.cn (C. Yan); tqian@suda.edu.cn (T. Qian)

A new approach using polypyrrole as nitrogen source has been demonstrated for the fabrication of nitrogen-doped graphene, which is subsequently served as nucleation centers for the growth of metal oxides. The thin layers of the nitrogen-doped graphene are not only used as the conductive pathways accelerating the electrical conductivity of the metal oxides but also served as buffer layers to improve the electrical contact with metal oxides nanostructures during the delithiation/lithiation of lithium ions. As anodes for lithium ion batteries, the nitrogen-doped graphene and their hybrids with MnO_2 nanorods exhibit exceptionally excellent capacity retention of 3000 cycles at 2500 mA g^{-1}, and ultrafast rate capability, which paves the way for developing electrode materials for long cycle-life energy storage devices.

KEYWOEDS: Nitrogen-doped graphene; Polypyrrole; Lithium ion battery; Anode materials; Ultralong cycle-life

Introduction

Nitrogen-doped graphene, a kind of graphene derivatives, exhibits excellent reliability, high capacity and fast lithium storage properties. In addition, N-doped structure can adjust the band structure of graphene without reducing conductivity.[1-3] Further studies reveal that the certain nitrogen doping seems to be the most appropriate method for strengthening the surface wettability of materials, capacity, and electronic conductivity while maintaining the superior cycle capability.[4] Rare methods have been discovered to prepare N-doped graphene, including chemical vapor deposition (CVD),[4] heating graphene with nitrogen rich compounds,[5] annealing graphite oxide (GO) in NH_3 and so on.[6] Among them, CVD is the most common method to synthesize N-doped graphene by making use of methane (CH_4) as the carbon source and NH_3[7] or pyridine[8] as nitrogen source via depositing on the nickel or copper substrate at a high temperature of 1000 °C. It's worth noting that metal impurities may be doped into N-doped graphene to affect materials real performance. Moreover, the use of CH_4, H_2, NH_3 and pyridine at high temperature is poisonous and dangerous. To address above issues, we report the novel method using polypyrrole (PPy) as N source for the fabrication of high-quality N-doped graphene.

Graphene based materials have been widely used in many fields, such as energy, electronics, biology, and catalysis[9-11] due to their excellent electric transport properties, distinguished conductivity, large surface area, and chemical properties. Lithium ion batteries are integral power sources in several current technologies.[12] With the development of the electronic products and electric vehicles, much progress

has been made to pursue the fast charging and discharging rates for lithium ion batteries.[13, 14] Various transition-metal oxides, such as Co_3O_4, [15] NiO, [16] MnO_2, [17, 18] MoO_2, [19] TiO_2[20] and V_2O_5, [21] have been widely used in lithium-ion batteries. They are confirmed to have ultrahigh values in energy density because of their unique conversion reactions.[22]Among all of transition metal oxides, manganese oxide (MnO_2), which is natural-abundant, cost-effective and environment-harmonious, has been known as promising electrode materials for lithium-ion batteries.[23-25] However, the problems of large volume changes and particulate matter aggregation during the process of intercalation and de-intercalation of the lithium ions result in poor cycling stability and low electrical conductivity (10^{-5}-10^{-6} S cm^{-1}).[26-29] To solve these problems, it is keen to find electrode materials which could promote the electron and ion diffusion coefficient simultaneously. Up to now, the results have been reported about the different kinds of MnO_2 nanostructure/graphene composites. As reported by Li et al., MnO_2 nanostructures grown on the graphene sheets only afforded a low capacity of 230 mA h g^{-1} at a current density of 200 mA g^{-1} after 150 cycles.[30] Yu et al. showed that the graphene-MnO_2 nanotube material exhibits a low capacity of 100 mA h g^{-1} at a current density of 495 mA g^{-1}.[31] Sun et al. reported that MnO_2 hierarchical nanostructures deliver a rise capacity of 381 mA h g^{-1} at the rate of 100 mA g^{-1} between 0.02 and 3.20 V.[18] However, it is critically important for lithium ion batteries to have long cycling life, high energy and power densities at rapid charge and discharge rates.

In the present work, a novel concept of synthesizing N-doped graphene has been

demonstrated using polypyrrole (PPy) as N source. Graphene oxide (GO) is in cocoon by PPy *via* in situ polymerization (PPy/GO), and during the carbonization process, N atoms in pyrrole rings may be easy to be converted to the N atoms in GO, which earns higher content of nitrogen (about 5.04 at%) than the previous methods.[32-34] Then MnO_2 nanorods decorated with N-doped graphene (MnO_2/NG) are fabricated facilely through solution-based reaction. N-doped graphene strengthens the performance of the ion and electron diffusions within the hybrid electrodes, resulting in high electronic conductivity. Furthermore, the excellent mechanical flexibility of N-doped graphene layers provides space for MnO_2 nanorods for volume accommodation during repeatable cycling process, which eventually results in enhanced cycle ability at ultrafast charge-discharge rate.

Experimental Section

Synthesis of the N-doped graphene

The graphene oxide (GO) was synthesized using modified Hummer's method.[34] The PPy/GO was prepared by the addition of 2.5 ml H_2O_2 to the GO/pyrrole/$FeCl_2$/H_2O (100 mg/0.5 ml/0.05 g/100 ml) mixture and lasted for 6 hours. Then, the PPy/GO was annealed in a quartz tube under the protection of the N_2 atmosphere (150 sccm) with a heating rate of 10 $^{\circ}$C min^{-1} to a carbonization temperature (500 °C, 700 °C, 900 °C, and 1100 °C each for 2 h) to prepare N-doped graphene nanosheets.

Synthesis of the MnO_2/NG composite

The MnO_2/NG composite was prepared by hydrothermal synthesis method. The reaction solution was obtained by mixing 11 mg $KMnO_4$ and 8 mg N-doped graphene nanosheets in 10 mL of deionized water under adequate stirring and then transferred into teflon-lined stainless steel autoclave. The autoclave was maintained at 220 °C for 24 h, then cooled down to room temperature.

General Characterization

Field emission scanning electron microscope (FESEM) imaging and field emission transmission electron microscope (FETEM) were performed on the SU8010, Hitachi, Ltd and the FEI Tecnai G220, FEI NanoPorts, Ltd. Surface elemental analysis was performed on the x-ray photoelectron spectrometer (XPS, Kratos Axis Ultra Dld, Japan) and the Powder X-ray Diffractometer (XRD, X'Pert-Pro MRD, Philips). Thermogravimetric Analysis (TGA, SDT 2960, USA) was performed on SDT 2960, TA Instruments. The elemental analysis was performed by Vario MICRO CUBE (Elementar Analysensysteme GmbH).

Electrochemical Characterization.

The working electrodes were prepared by making thoroughly mixed by 70 wt% active materials, 20 wt% acetylene black, and 10 wt% polytetrafluoroethylene (PTFE, 60 wt% dispersion in water) on the Titanium foil (0.1mm). After dried in vacuum at 60 ℃ for 6 h, the battery was made in Glove box (Shanghai Mikrouna Mech. Tech. Co., Ltd), where the electrolyte was $LiPF_6$ (1M) in ethylene carbonate (EC) and dimethyl carbonate (DMC) (1:1, v/v). The galvanostatic charge-discharge properties and cyclic voltammetric were tested in the voltage range of 0.0~3.0 V on the

CT2001A cell test instrument (Wuhan LAND Electronic Co., Ltd) and CHI 660E (Shanghai Chenhua instrument Co., Ltd) electrochemical workstation, respectively.

Results and Discussion

Our controlled synthesis of the MnO_2/NG hybrids is illustrated in Scheme 1. GO sheets are coated with PPy layers by π-π and electrostatic interactions through *in-situ* polymerization. As the neighbor of C in the periodic table, the N atoms in pyrrole rings may be easily converted to N atoms in GO via PPy's decomposition and recasting in the carbonization process.[6,35] The prepared N-doped graphene then served as nucleation centers for the deposition of MnO_2 nanorods, which can be described as follows:[30, 36]

$$MnO_4 + C + H \rightarrow MnO_2 + CO_2 + H_2O$$

The general structure, size and morphology of MnO_2/NG composite were investigated by scanning electron microscopy (SEM) and transmission electron microscopy (TEM) (Fig. 1). It is obvious that the dense PPy/GO nanostructures (Fig. S1A) become thin and transparent nanosheets with 3D structures (N-doped graphene, Fig. S1B) after carbonization. The sufficient distance between nanosheets is loose and suitable for the growth of MnO_2 nanorods. It can be seen (Fig. 1A and 1B) that each of MnO_2 nanostructures is nanorod-shaped, which has several micrometers in length and grows on the surface of N-doped graphene uniformly. Fig. 1C shows TEM image of deposited MnO_2 nanorods with an average diameter about 108 nm. For more details, the crystalline nature of MnO_2 nanorods is presented in Fig. 1D, which reveals a crystal lattice space of 0.35 nm for the crystalline MnO_2 nanostructures.

X-ray diffraction (XRD) pattern of MnO_2/NG samples was displayed in Fig. 2A. Board and strong peaks around 44.5 ° and 26 ° are observed, arising from (002) and (100) crystal planes of N-doped graphene. The peaks located at 65.5 °, 44.3 °, 42.6 °, 38.8 °, 34.4 °, 32.8 °, and 28.8 ° belong to the (002), (521), (131), (031), and (310) planes of MnO_2. All the diffraction peaks of the assembled MnO_2/NG correspond to individual N-doped graphene and MnO_2 nanostructure indices. X-ray photoelectron spectroscopy (XPS) analysis was investigated to identify the chemical component of the as-prepared product. From careful inspection of wide region spectroscopy and elemental analysis, the characteristic signals attributed to C, N, O, and Mn can be observed distinctly (Fig. 2B), which reveal the existence of N and Mn components. Fig. S2 shows the high-resolution XPS spectra for C, N, O and Mn. The core level peak of C1s can be resolved into three components centered at 284.7 eV, 285.3 eV, and 286.3 eV[37] (Fig. S2A) representing sp^2C-sp^2C, N-sp^2C and N-sp^3C bonds, respectively. In addition, it could be observed that the spectrum of N1s is resolved into three components centered at 389.9 eV, 401.2 eV (Fig. S2B), and 402.7 eV,[37] corresponding to pyridinic N, pyrrolic N, and graphitic N (Fig. 2C), which indicate the existence of N-doped graphene. The peaks represent $Mn2p_{3/2}$ and $Mn2p_{1/2}$ centered at 642.2 eV and 653.8 eV (Fig. S2C),[17] while the peaks represent O-Mn and O-C at 530.4 eV and 531.7 eV (Fig. S2D),[25] confirming the present of MnO_2 in the composite synergistically. Moreover, thermo gravimetric analysis (TGA) (Fig. 2D) demonstrates that the weight loss of the MnO_2/NG composites is around 68.78 % at 800 ℃, revealing that the content of MnO_2 in the MnO_2/NG is 31.22 %.

To express the unique superiority of electrochemical properties of the MnO_2/NG, electrodes were directly investigated using half cells versus Li/Li^+. Cyclic voltammetry (CV) was used to analyze the charge storage behaviors at a slow scan rate of 0.6 mV s^{-1} between 0.01V and 3V. From the first cycle of Fig. 3A, it is clear that the curve in the first process is different from the subsequent ones. The peak at 0.35 V in the first cycle is assigned to the characteristic of the solid electrolyte interface (SEI) formation on the electrode surface and the reduced reaction of the MnO_2 and Li ions. The electrochemical oxidation reaction of solid electrolyte interface layers can be proved by two oxidation peaks at 1.3 V and 2.3 V. After the first cycle, it is obviously observed the peaks of the follow-up curves are nearly unchanged, which demonstrates excellent structural stability and electrochemical reversibility of the MnO_2/NG. The electrochemical performance had been further examined by representative discharge-charge voltage profiles at 1C (1C = 1000 mA g^{-1}) between 0 and 3 V (Fig. 3B). The initial discharge and charge capacities are found to be 1410.6 mA h g^{-1} and 780.0 mA h g^{-1}. The capacity loss may be caused by SEI formation as well as decomposition of electrolyte during the first electrochemical reaction. This characteristic is also consistent well with the peaks appearing in the first scan while disappearing afterward in CV curves. The discharge voltage plateau at 0.28V in the first discharge process is different from the plateau of other cycles at 0.41V, which points out that the irreversible reactions happened in the first cycle process. During the next cycles of the charge and discharge process, the plateaus at

the 0.41V are nearly unchanged, further indicating that the electrode of MnO_2/NG mixture has excellent stable performance.

The cycling performance for MnO_2/NG was evaluated in the potential window of 0 to 3 V (Fig. 3C). At a current density of 100 mA g^{-1}, the discharge capacity tends to stabilize about 647.5 mA h g^{-1} after fifth cycles and rise slowly. Moreover, the MnO_2/NG battery was evaluated by galvanostatic discharge/ charge at various current rates. From Fig. 3C, it can be seen that the discharge capacity varies from 607.5 mA h g^{-1}, 511.7 mA h g^{-1}, 415.5 mA h g^{-1}, 320.7 mA h g^{-1}, 253.4 mA h g^{-1}, 212.0 mA h g^{-1}, 184.9 mA h g^{-1}, 163.3 mA h g^{-1}, 143.1 mA h g^{-1}, 104.4 mA h g^{-1}, 94.4 mA h g^{-1}, 90.0 mA h g^{-1} with the increasing current rate from 0.1C, 0.2C, 0.4C, 0.8C, 1.6C, 2.4C, 3.2C, 4C, 5C, 8C, 10C, 12C. The capacity then increases back to 286.7 mA h g^{-1}, 375.6 mA h g^{-1}, and 638.6 mA h g^{-1} when the current rate returns to 1.6C, 0.8C, and 0.1C. By returning to the initial rate of 100 mA g^{-1}, the discharge capacity could almost return back to the original capacity, which can further demonstrate the elite performance of the fast and efficient transport of ions/electrons. By contrast, the pure MnO_2 electrode exhibits low discharge capacities, which illustrate that the improved rate performance is most likely due to the superior electronic conductivity for the N-doped graphene.

To ensure a fair comparison of the excellent stability, the electrochemical performance was investigated at a current rate of 300 mA g^{-1} (Fig. 3D). The reconstituted N functional groups of N-doped graphene sheets are vital for improving their redeposition process upon discharge/charge. Also, the discharge/charge process

show perfect cycling stability and relatively high specific capacity during the 200th cycles. In addition, the Coulombic efficiency of the anode retains nearly 100% since the second cycle, further indicating its excellent reversibility. The electrochemical impedance spectroscopy (EIS) measurements were shown in the Fig. 3E, which can further explain the superior electrochemical performance. Due to excellent electrical conductivity and the surface capacitive effects of N-doped graphene, charge transfer and inherent resistances of the MnO_2/NG's are lower than those of bare MnO_2 electrodes, indicating superior conductivity which is beneficial for the rate capability enhancement. Furthermore, the MnO_2/NG composites are then tested at a high current density of 2500 mA g^{-1} (Fig. 3F), where the capacity retention can reach almost 100% after 3000 cycles, further confirming the extremely long cycle-life of lithium ion batteries.

Conclusions

In summary, we present a novel and facile approach for fabricating high quality N-doped graphene, which can easily command the surface attractive force of the local electronic structures and enhance binding with Li-ions. The sufficient distance between each N-doped graphene sheets are suitable for volume accommodation of the MnO_2 electrode during ultrafast charge-discharge process. The as-prepared N-doped graphene/MnO_2 electrode battery exhibits ultralong cycle life exceeding 3000 cycles (at a current density of 2500 mA g^{-1}) and remarkable reversible capacity of 638.6 mA h g^{-1} at a current density of 100 mA g^{-1}, which provides wide potential of application to meet the high performance requirements of power sources.

Acknowledgements

We acknowledge the support from the "Thousand Talents Program", the Natural Science Foundation of Jiangsu Province of China (no.BK20140315), the National Natural Science Foundation of China (no. 51402202), the National Basic Research Program of China (no. 2015CB358600), the Jiangsu Shuangchuang Plan, and the Priority Academic Program Development of Jiangsu Higher Education Institutions (PAPD).

Notes and References

1. Y. Y. Shao, S. Zhang, M. H. Engelhard, G. S. Li, G. C. Shao, Y. Wang, J. Liu, A. I. Aksayc and Y. H. Lin, *J. Mater. Chem.*, **2010**, *20*, 7491.
2. Y. Z. Xue, B. Wu, Q. L. Bao and Y. Q. Liu, *Small*, **2014**, *10*, 2975.
3. Y. Ito, H. J. Qiu, T. Fujita, Y. Tanabe, K. Tanigaki and M. W. Chen, *Adv. Mater.*, **2014**, *26*, 4145.
4. L. F. Chen, X. D. Zhang, H. W. Liang, M. G. Kong, Q. F. Guan and P. Chen, *ACS Nano*, **2012**, *6*, 7092.
5. S. Gilje, S. Han, M. S. Wang, K. L. Wang and R. B. Kaner, *Nano Lett.*, **2007**, *7*, 3394.
6. Z. Q. Luo, S. H. Lim, Z. Q. Tian, J. Z. Shang, L. F. Lai, B. MacDonald, C. Fu, Z. X. Shen, T. Yu and J. Y. Lin, *J. Mater. Chem.*, **2011**, *21*, 8038.
7. N. Li, Z. Y. Wang, K. K. Zhao, Z. J. Shi, Z. N. Gu and S. K. Xu, *Carbon*, **2010**, *48*, 255.

8. L. S. Panchakarla, K. S. Subrahmanyam, S. K. Saha, A. Govindaraj, H. R. Krishnamurthy, U. V. Waghmare and C. N. R. Rao, *Adv. Mater.*, **2009**, *21*, 4726.
9. T. Qian, C. F. Yu, S. S. Wu and J. Shen, *J. Mater. Chem. A*, **2013**, *1*, 6539.
10. F. Withers, T. H. Bointon, M. F. Craciun and S. Russo, *ACS Nano*, **2013**, *7*, 5052.
11. S. Borini, R. White, D. Wei, M. Astley, S. Haque, E. Spigone, N. Harris, J. Kivioja and T. Ryhanen, *ACS Nano*, **2013**, *7*, 11166.
12. B. Kang and G. Ceder, *Nature*, **2009**, *458*, 190.
13. H.G. Zhang, X.D. Yu and P.V. Braun, *Nat. Nanotechnol.*, **2011**, *6*, 277.
14. Y. C. Qiu, W. F. Li, W. Zhao, G. Z. Li, Y. Hou, M. N. Liu, L. S. Zhou, F. M. Ye, H. F. Li, Z. H. Wei, S. H. Yang, W. H. Duan, Y. F. Ye, J. H. Guo and Y. G. Zhang, *Nano Lett.*, **2014**, *14*, 4821.
15. W. Y. Li, L. N. Xu and J. Chen, *Adv. Funct. Mater.*, **2005**, *15*, 851.
16. S. A. Needham, G.X. Wang and H. K. Liu, *J. Power Sources*, **2006**, *159*, 254.
17. L. Li, A. O. Raji and J. M. Tour, *Adv. Mater.*, **2013**, *25*, 6298.
18. D. F. Sun, J. T. Chen, J. Yang and X. B. Yan, *CrystEngComm*, **2014**, *16*, 10476.
19. C. B. Zhu, X. K. Mu, P. A. Aken, J. Maier and Y. Yu, *Adv. Energy Mater.*, **2014**, *DOI: 10.1002/aenm.201401170*.
20. W. X. Guo, X. Y. Xue, S. H. Wang, C. J. Lin and Z. L. Wang, *Nano Lett.*, **2012**, *12*, 2520.
21. T. Qian, N. Xu, J. Q. Zhou, T. Z. Yang, X. J. Liu, X. W. Shen, J. Q. Liang and C. L. Yan, *J. Mater. Chem. A*, **2015**, *3*, 488.

22. P. P. S. Laruelle, S. Grugeon, L. Dupont and J. M. Tarascon, *Nature,* **2000**, *407*, 496.

23. J. Cabana, L. Monconduit, D. Larcher and M. R. Palac ń, *Adv. Mater*., **2010**, *22*, E170.

24. L. F. Chen, Z. H. Huang, H. W. Liang, Q. F. Guan and S. H. Yu, *Adv. Mater*., **2013**, *25*, 4746.

25. Z. S. Wu, W. C. Ren, D. W. Wang, F. Li, B. L. Liu and H. M. Cheng, *ACS Nano*, **2010**, *4*, 5835.

26. X. Y. Lang, A. Hirata, T. Fujita and M. W. Chen, *Nat. Nanotechnol*., **2011**, *6* , 232

27. X. Y. Han, F. Zhang, Q. F. Meng and J. T. Sun, *J. Am. Ceram. Soc*., **2010**, *93*, 1183.

28. L. Y. Yuan,; X. H. Lu, X. Xiao, T. Zhai, J. J. Dai, F. C. Zhang, B. Hu, X. Wang, L. Gong, J. Chen, C. G. Hu, Y. X. Tong, J. Zhou and Z. L. Wang, *ACS Nano*, **2012**, *6*, 656.

29. H. Lai, J. X. Li, Z. G. Chen and Z. G. Huang, *ACS Appl. Mater. Interfaces*, **2012**, *4*, 2325.

30. J. X. Li, Y. Zhao, N. Wang, Y. H. Ding and L. H. Guan, *J. Mater. Chem*., **2012**, *22*, 13002.

31. A. P. Yu, H. W. Park, A. Davies, D. C. Higgins, Z. G. Chen and X. C. Xiao, *J. Phys. Chem. Lett.,* **2011**, *2*, 1855.

32. F. H. Du, B. Li, W. Fu, Y. J. Xiong, K. X. Wang and J. S. Chen, *Adv. Mater*., **2014**, *26*, 6145.

33. T. Qian, C. F. Yu, S. S. Wu and J. Shen, *Biosens. Bioelectron*., **2013**, *50*, 157.

34. Jr. W.S. Hummers and R.E. Offeman, *J. Am. Chem. Soc*., **1958**, *80*, 1339.

35. X. R. Wang, X. l. Li, L. Zhang, Y. k. Yoon, P. K. Weber, H.l. Wang, J. Guo and H.J. Dai, *Science*, **2009**, *324,768*.

36. J. X. Li, N. Wang, Y. Zhao, Y. H. Ding and L. H. Guan, *Electrochem. Commun.* , **2011**, *13, 698*.

37. A. L. M. Reddy, A. Srivastava, S. R. Gowda, H.Gullapalli, M. Dubey, and P. M. Ajayan, *Acs Nano*, **2010**, *4, 6337*.

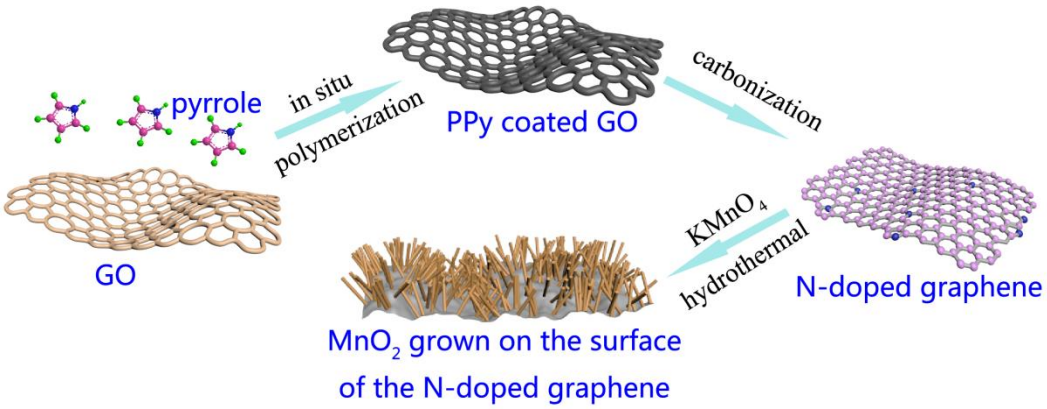

Scheme 1. Schematic representation of the preparation of the PPy/GO, N-doped graphene, and MnO_2/NG hybrids.

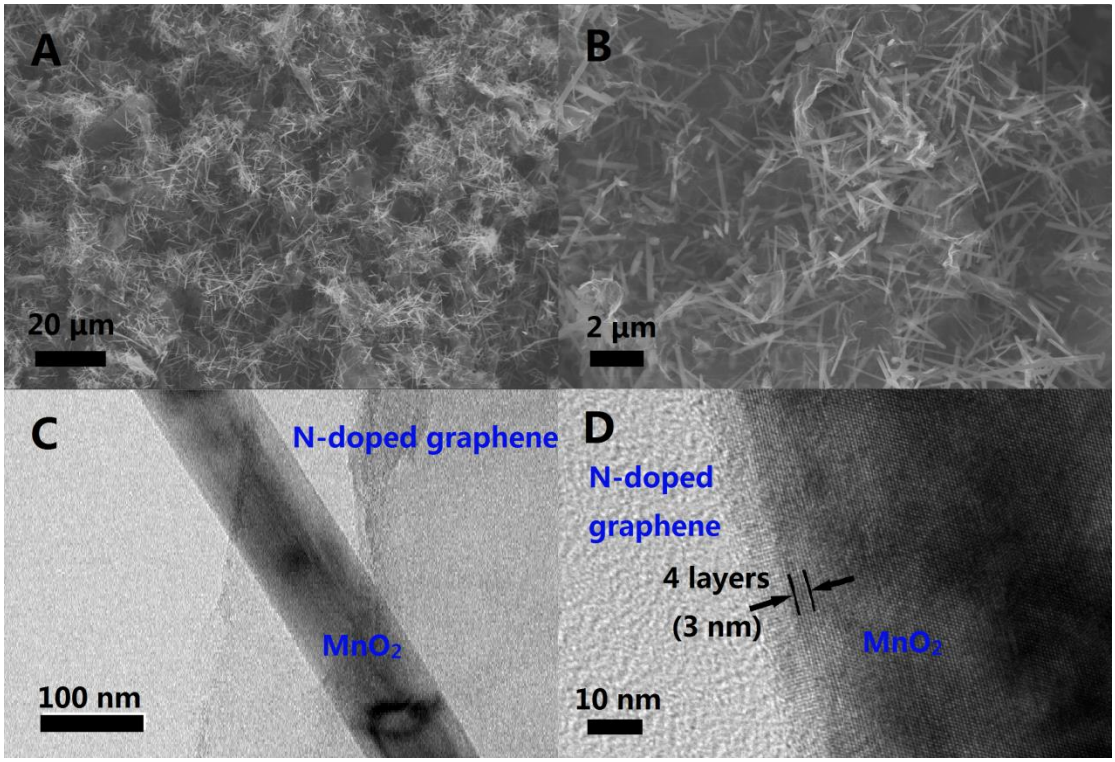

Fig. 1. (A) Low-magnification and (B) High-magnification SEM images of MnO_2 nanorodes grown on the N-doped graphene sheets; (C) TEM image of MnO_2/NG; (D) High resolution TEM of MnO_2/NG with partial enlarged.

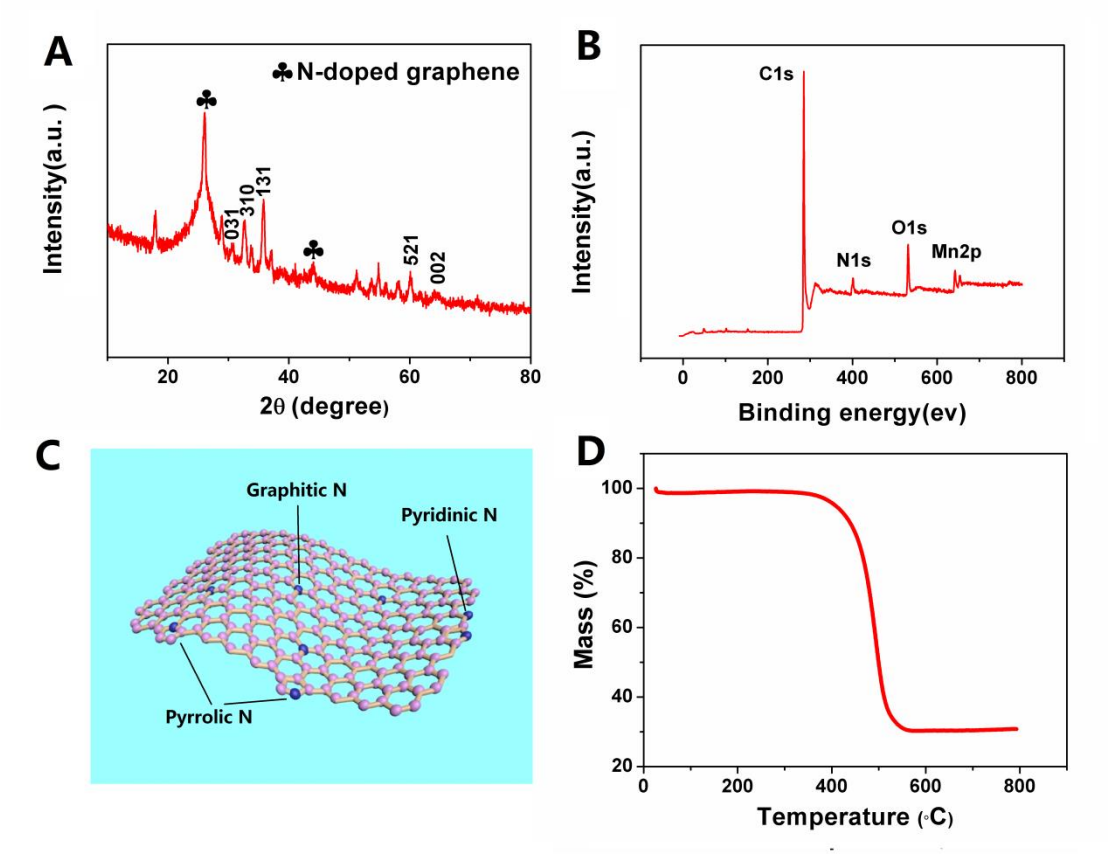

Fig. 2. (A) XRD pattern and (B) XPS spectrum of MnO_2/NG. (C) The explanatory diagram of the different N functionalities in the N-doped graphene. (D) The TGA between 0 °C and 800 °C at an increasing rate of 10°C min^{-1}.

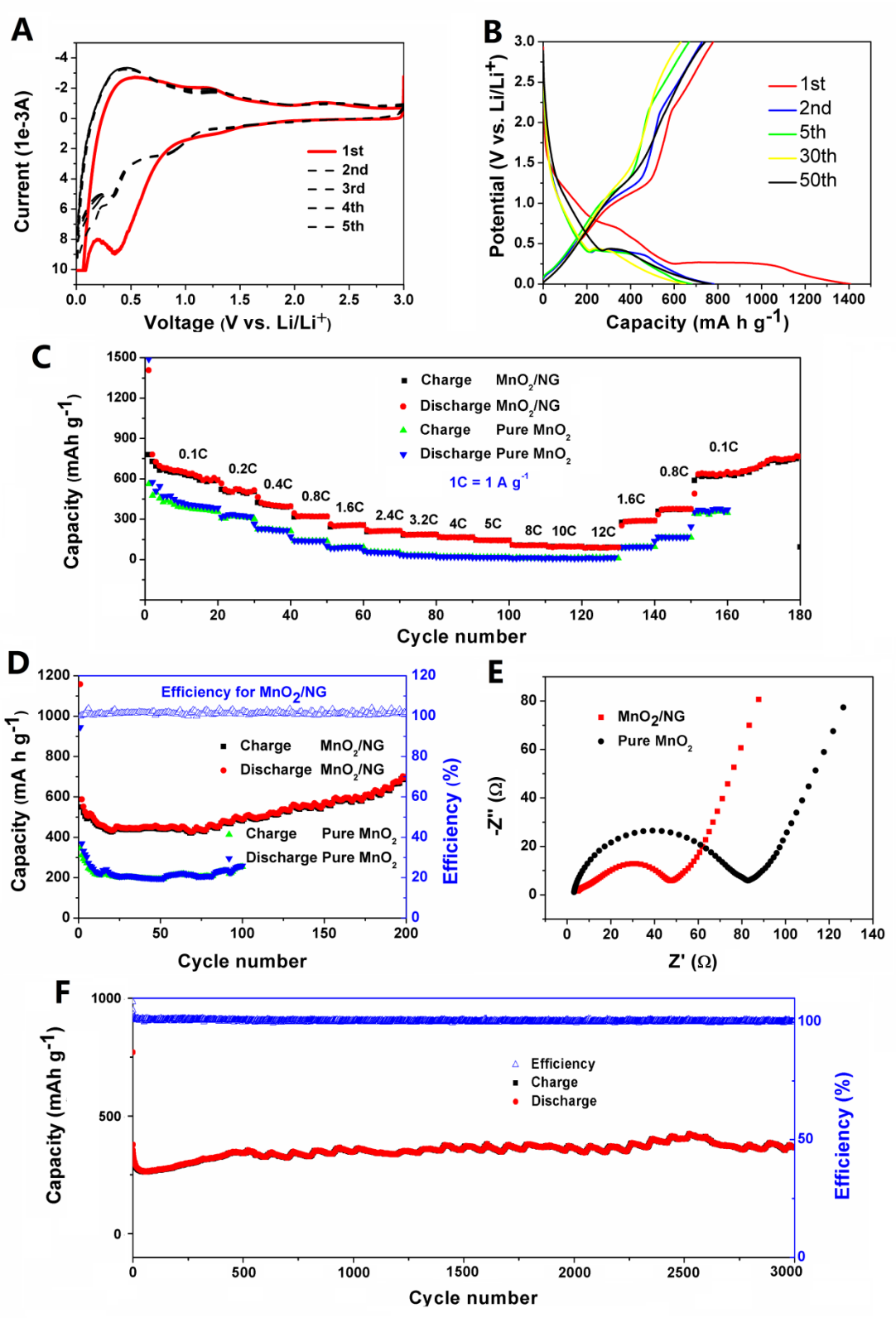

Fig. 3.(A) The foundation test of the electrochemical properties by the cyclic voltammetry obtained at a voltage range of 0.01 to 3V (vs Li^+/Li) and potential scan rate of 0.6 mV s^{-1}.(B) Galvanostatic charge/discharge profile for the first, second, fifth,

tenth, and fiftieth cycles of the MnO_2/NG anode at the current density of 100 mA g^{-1}. (C) Rate performance of the MnO_2/NG composite and pure MnO_2. (D) Cycling performance of MnO_2/NG anode and pure MnO_2 at a current density of 300 mA g^{-1}, and the efficiency is plotted on the right axis. (E) Nyquist plots of the MnO_2/NG and bare MnO2 anode at the fresh coin cells over the frequency range from 0.1Hz to 100 kHz. (F) Long-term cycling performance of the MnO_2/NG anode at a high current density of 2500 mA g^{-1}, and the efficiency is plotted on the right axis (blue circles).